# SUPPORTING INFORMATION

for

# Catalyst-Free Dynamic Transesterification towards High-Performance and Fire-Safe Epoxy Vitrimer and Its Carbon Fiber Composite

Jia-Hui Chen, Bo-Wen Liu, Jia-Hui Lu, Peng Lu, Ya-Ling Tang, Li Chen* and Yu-Zhong Wang

*The Collaborative Innovation Center for Eco-Friendly and Fire-Safety Polymeric Materials (MoE), National Engineering Laboratory of Eco-Friendly Polymeric Materials (Sichuan), State Key Laboratory of Polymer Materials Engineering, College of Chemistry, Sichuan University, Chengdu 610064, China.*

**Corresponding to: l.chen.scu@gmail.com (L. Chen)*

**Table of Contents**

## 1. Experimental section

### 1.1 Materials

Diglycidyl ether of bisphenol A (DGEBA, DER 332) was procured from Sigma-Aldrich (St. Louis, MO, USA); adipic acid (AA, 99%) was purchased from Adamas Pharmaceuticals, Inc. (Shanghai, China); 10-(2,5-dihydroxyphenyl)-10H-9-oxa-10-phospha-phenantbrene-10-oxide (DOPO-HQ, 99%) was provided by Guangzhou Xi Jia New Materials Co., Ltd. 1,4-Bis(2-hydroxyethoxy) benzene (HQEE, >95%) and potassium iodide (KI, 99%) were purchased from Aladdin Industrial Co., Ltd. (Shanghai, China); ethylene carbonate was supplied by Adamas Pharmaceuticals, Inc. (Shanghai, China); N,N-dimethylacetamide (DMAc) was purchased from Zhiyuan Chemical Reagent Co., Ltd. (Tianjin, China); chloroform ($CHCl_3$) was obtained from Kelong Chemical Reagent Co., Ltd. (Sichuan, China); ethylene glycol (EG) was obtained from Aladdin Industrial Co., Ltd. (Shanghai, China) with a purity of 99.9%. Unidirectional TC35R-12K carbon fibers (CFs) were produced by TAIRYFIL. All materials were used directly as received without further purification.

### 1.2 Preparation of DOPO-HQ-HE (DHH)

The preparation of DOPO-HQ-HE (DHH) has been reported in previous literature.[1]10-(2,5-dihydroxyphenyl)-10H-9-oxa-10-phospha-phenantbrene-10-oxide (DOPO-HQ) (64.8 g, 0.2 mol), ethylene carbonate (52.8 g, 0.6 mol), KI (0.8 g) and DMAc (100 g) were mixed into a round-bottom glass flask equipped with a nitrogen inlet, a condenser, and a magnetic stirrer. The flask was heated to 160 °C and then maintained for 8 h until the reaction without producing bubbles. Then, the reaction mixture was poured into quantitative distilled water, resulting in the precipitation of yellow powders. Next, the filter residue was washed with distilled water several times. Recrystallization from methyl alcohol was carried out if needed (78.1% yield). $^1$H NMR (400 MHz, DMSO-$d_6$), δ 8.30-8.20 (m, 2H), 7.77 (ddt, 1H), 7.68 (ddd, 1H), 7.57-7.42 (m, 2H), 7.41-7.27 (m, 3H), 7.20 (dd, 1H), 7.03 (dd, 1H), 4.87 (t, J = 5.5 Hz, 1H), 4.46 (t,1H), 4.05-3.90 (m, 2H), 3.69 (dt, 3H), 3.55 (dt, 1H), 2.96 (qd, 2H). $^{31}$P NMR (400 MHz, DMSO-$d_6$), δ 20.37. Melting point, 162-166 °C.

### 1.3 Characterization

Fourier transform infrared spectroscopy (FT-IR) was recorded on a NICOLET 6700 FTIR spectrometer (Thermo Electron Corporation, USA) from 4000 to 500 $cm^{-1}$ with a resolution and scanning time of 4 $cm^{-1}$ and 32, respectively. The electron binding energy of P2p was analyzed by X-ray photoelectron spectroscopy (XPS) (Thermo Fisher Scientific, USA) with Al Kα excitation radiation. The gel fraction and swelling measurements were conducted following the immersion method in 25 mL of $CHCl_3$ for 7 days at room temperature. The gel fraction is defined as $m_2/m_0$ and swelling ratio is determined as $m_1/m_2$, where $m_0$ is the weight of the sample before swelling, $m_1$ is the mass of the swollen sample and $m_2$ is the insoluble part.

The curing behavior and the glass transition temperature ($T_g$) of the samples were monitored by differential scanning calorimetry (DSC, TA Q200). The samples (~2.0 mg) were scanned from 40 to 300 °C at a heating rate of 10 °C·$min^{-1}$ under a $N_2$ atmosphere. To investigate the curing kinetics of AAD-EP in the presence of DHH as multifunctional modifier, each sample was scanned at different heating rates (5, 10, 15, and 20 °C·$min^{-1}$). The activation energy was calculated based on the Kissinger and Ozawa method.[2] The thermal stability of AAD-EP was examined by using thermogravimetric analysis (TGA, TA 5500). The samples (~5.0 mg) were heated from 40 to 700 °C at a heating rate of 10 °C·$min^{-1}$ under a $N_2$ and air atmosphere. The dynamic mechanical properties were tested on the dynamic mechanical analysis (DMA) (Q800, TA instrument) via a tensile resonant mode. The samples were scanned from -30 to 150 °C at a heating rate of 5 °C·$min^{-1}$, with an oscillating amplitude of 10 μm and a frequency of 1 Hz.

The tensile test was performed on a CMT2000 universal testing machine at room temperature (~25 °C) with a crosshead speed of 1 mm·$min^{-1}$ according to ASTM D638. The standard dumbbell-shaped samples had dimensions of 75 × 5 × 2 $mm^3$, and the gauge length between the two pneumatic grips was 25 mm. At least five repeats were performed for each sample. The three-point short beam flexural strength was tested according to GB/T 3356-2014. The standard samples had dimensions of 100 × 10 × 2 $mm^3$.

Fire safety was evaluated by the limiting oxygen index (LOI) and Underwriter Laboratory 94 vertical burning tests (UL-94 V). The LOI tests were conducted with sample dimensions of 130 mm × 6.5 mm × 3.2 mm, according to ASTM D2863, and measured on an HC-2C oxygen index meter (Jiangning Analysis Instrument Company, China). The UL-94 V burning rating tests were performed with sample dimensions of 130 mm × 13 mm × 3.2 mm, according to ATSM D3801, and measured on a CZF-2 instrument (Jiangning, China). The combustion behavior was obtained with a cone calorimeter (Fire Testing Technology, UK) according to ISO 5660. Samples with dimensions of 100 mm × 100 mm × 3 mm were exposed to a radiant cone under a heat radiation of 35 $kW \cdot m^{-2}$, while the composites with dimensions of 100 × 100 × 3.2 mm were exposed to a radiant cone under a heat radiation of 50 $kW \cdot m^{-2}$.

The morphological features of the char residues after cone calorimetry were observed by scanning electronic microscopy (SEM) (JEOL JSM 5900 LV, Japan), and EDX was employed to observe the elemental composition and distribution under the surface scanning model. The Raman spectra were investigated on a DXR2xi Raman spectrometer (Thermo Fisher Scientific, USA) with char residues (with a 532 nm laser line). TG-IR was carried out via TGA coupled with an FT-IR spectrometer at a heating rate of 20 $°C \cdot min^{-1}$ from 40 °C to 700 °C in a nitrogen atmosphere (flow rate: 25 $mL \cdot min^{-1}$).

Stress relaxation was performed on a dynamic rotational rheometer (ARES Rheometer, TA, USA). The specimens were put into the two plates of the equipment and heated to the experimental temperature for 10 min to reach thermal equilibrium. Then, a constant normal force of 5 N was applied to maintain good contact between the sample and parallel plates, 1% strain was loaded and maintained, and the relaxation modulus as a function of time was recorded. The repair property of AAD-EP was monitored by an optical microscope (Axio Scope.A1). The sample was scratched to create a crack on the surface using a knife, placed between two metal plates, and then placed in an oven at 200 °C for different times to observe the repair process.

The ESI mass spectra for MS of the degradation products were recorded on a TSQ Quantum Ultra LC-MS system in positive mode.

## 2. Curing formulation

Formulations of AA-EP and AAD-EP curing systems were summarized in Table S1; chemical structures of the different components, including DGEBA, AA, DHH and HQEE, were shown in Fig. S1.

**Table S1.** Formulations of AA-EP and AAD-EP curing systems.

| Sample | DGEBA | AA | DHH | | P content | HQEE | |
|---|---|---|---|---|---|---|---|
| | (g) | (g) | (g) | (wt %) | (wt %) | (g) | (wt %) |
| AA-EP | 1 | 0.43 | - | - | - | - | - |
| AAD0.25-EP | 1 | 0.43 | 0.30 | 17.34 | 1.30 | - | - |
| AAD0.5-EP | 1 | 0.43 | 0.61 | 29.90 | 2.25 | - | - |
| AAH0.5-EP | 1 | 0.43 | - | - | - | 0.29 | 16.86 |

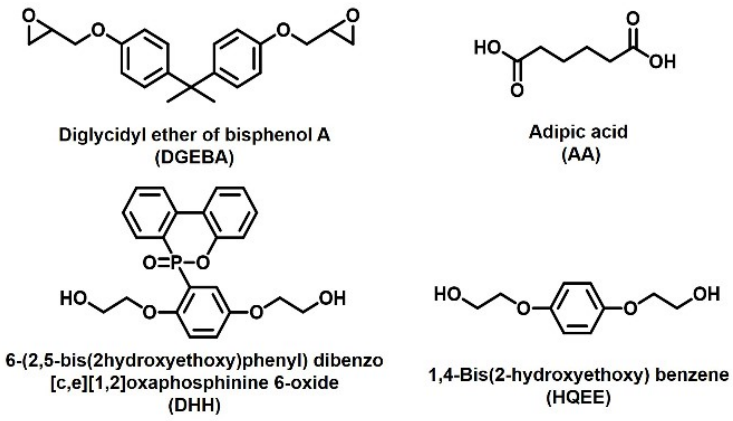


**Fig. S1** The chemical structures of DGEBA, AA and DHH, as well as the control sample HQEE.

## 3. Curing behavior

DSC heating curves of AAD-EP and AAD-EP at a heating rate of 10 °C·min$^{-1}$ were shown in Fig. S2. The nonisothermal curing behaviors with different heating rates from 5 to 20 °C·min$^{-1}$

were investigated (Fig. S3). All curves appeared obvious curing exothermic peak proved the occurrence of the curing process. Based on Kissinger's equation and Ozawa's equation,[2] the activation energy Ea and Ea′ of curing reaction was calculated from the linear fitting plots of $\ln(\beta/T_P^2)$ and $\ln \beta$ versus $1/T_p$, respectively. The calculated Ea and Ea′ of AA-EP was 102 kJ·mol$^{-1}$ and 89.2 kJ·mol$^{-1}$, respectively (the difference about value is resulted from different computational equation). When introducing DHH into the AA-EP, the Ea and Ea′ of AAD0.25-EP decreased to 82.1 kJ·mol$^{-1}$ and 70.5 kJ·mol$^{-1}$. With the DHH loading increased to AAD0.5-EP, the activation energy (Ea and Ea′) further decreased to 81.5 kJ·mol$^{-1}$ and 69.9 kJ·mol$^{-1}$. These results indicated that DHH was efficient in reducing the activation energy of the AAD-EP.

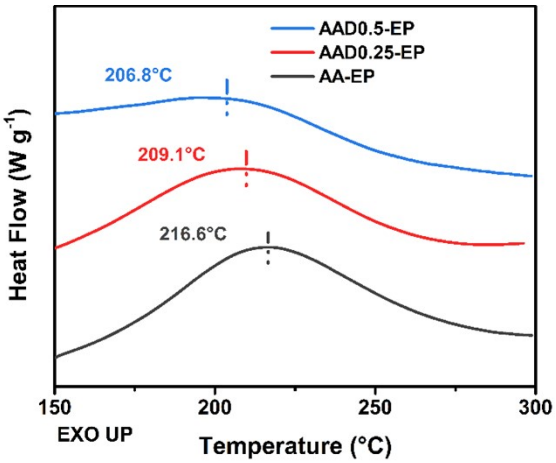


**Fig. S2** DSC heating curves of AAD-EP and AAD-EP at a heating rate of 10 °C·min$^{-1}$.

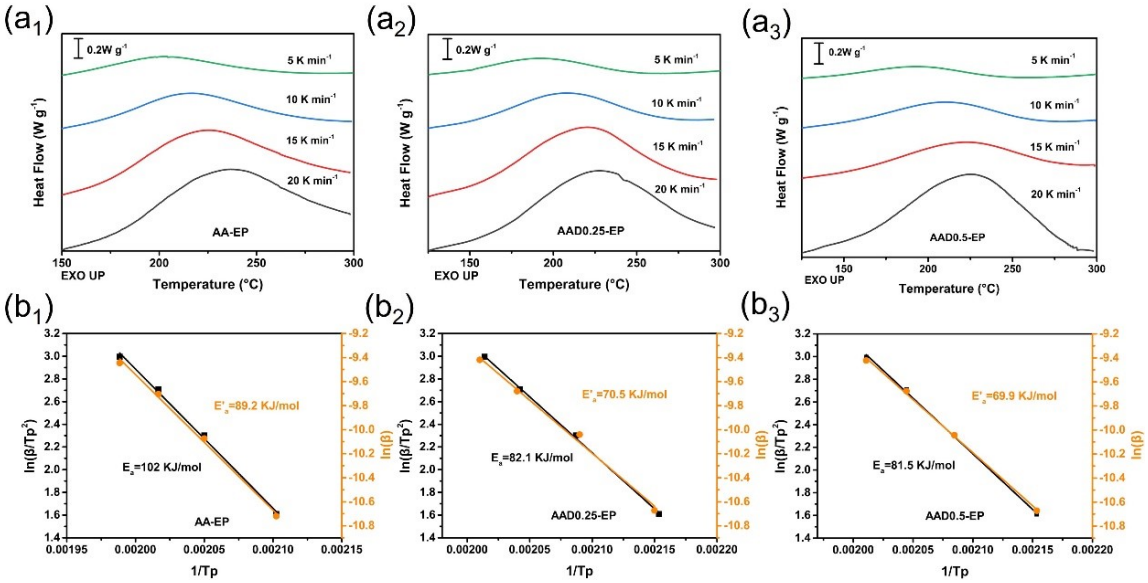


**Fig. S3** The non-isothermal DSC scanning with heating rates of 5, 10, 15 and 20 °C·min$^{-1}$ ($a_1$-$a_3$); the linear fitting plots of $\ln(\beta/T_P^2)$ and $\ln\beta$ versus $1/T_p$ based on Kissinger's equation and Ozawa's equation, respectively ($b_1$-$b_3$).

## 4. Fourier transform infrared spectroscopy (FT-IR)

FT-IR spectra of the EP monomer DGEBA, the curing agent AA, DHH, the cured samples AA-EP and AAD0.5-EP, were shown in Fig. S4.

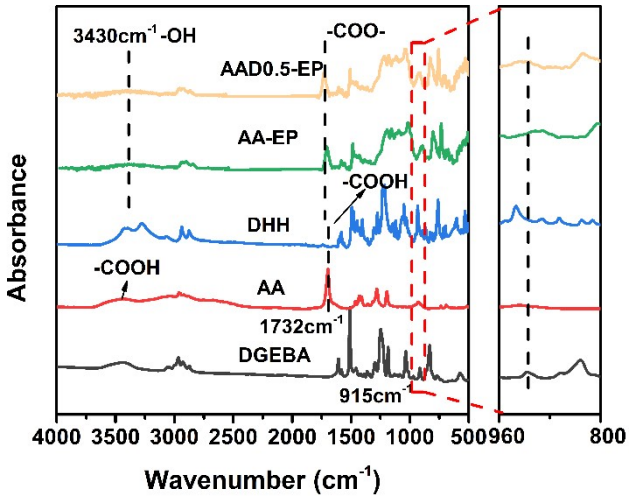


**Fig. S4** FT-IR spectra of DGEBA, AA, DHH, the cured AA-EP and AAD0.5-EP samples.

## 5. Gel fraction and swelling ratio

The gel fraction and swelling measurements were conducted following the immersion method in 25 mL of $CHCl_3$ for 7 days at room temperature. The gel fraction is defined as $m_2/m_0$ and swelling ratio is determined as $m_1/m_2$, where $m_0$ is the weight of the sample before swelling, $m_1$ is the mass of the swollen sample and $m_2$ is the insoluble part. All the compositions exhibited high gel content over 90%, indicating AAD-EP with complete cross-linked network. With the increase of DHH loading, the swelling ratio of the AAD-EP consistently increase, which was due to the rigid DHH structure resulting in the decrease of cross-linking density (Fig. S5).

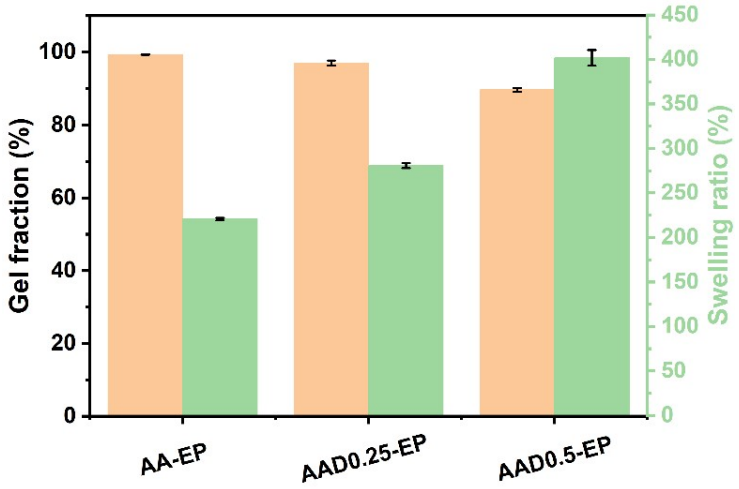


**Fig. S5** Gel fraction and swelling ratio of the cured AA-EP and AAD-EP samples.

## 6. Thermal property

Thermal analysis data from DMA of the cured AA-EP, AAD-EP and AAH0.5-EP samples were collected in Table S2.

**Table S2.** Thermal analysis data of AA-EP, AAD-EP and AAH0.5-EP.

| Sample | $E_g$[a] (MPa) | $T_\alpha$[b] (°C) | $T_g$ (°C) | $\nu_e$ (mol·m$^{-3}$) |
|---|---|---|---|---|
| AA-EP | 2906 | 91.3 | 72.3 | 1155.2 |

| | | | | |
|---|---|---|---|---|
| AAD0.25-EP | 2946 | 85.8 | 65.5 | 601.4 |
| AAD0.5-EP | 3179 | 94.4 | 65.7 | 225.1 |
| AAH0.5-EP | 2279 | 68.6 | 36.9 | 520.0 |

[a] Represents the storage modulus at 25 °C; [b] represents the peak temperature of tan δ.

## 7. Thermogravimetric Analysis

TG and DTG curves of the cured AA-EP, AAD-EP and AAH0.5-EP samples in $N_2$ and air atmospheres were shown in Table S2.

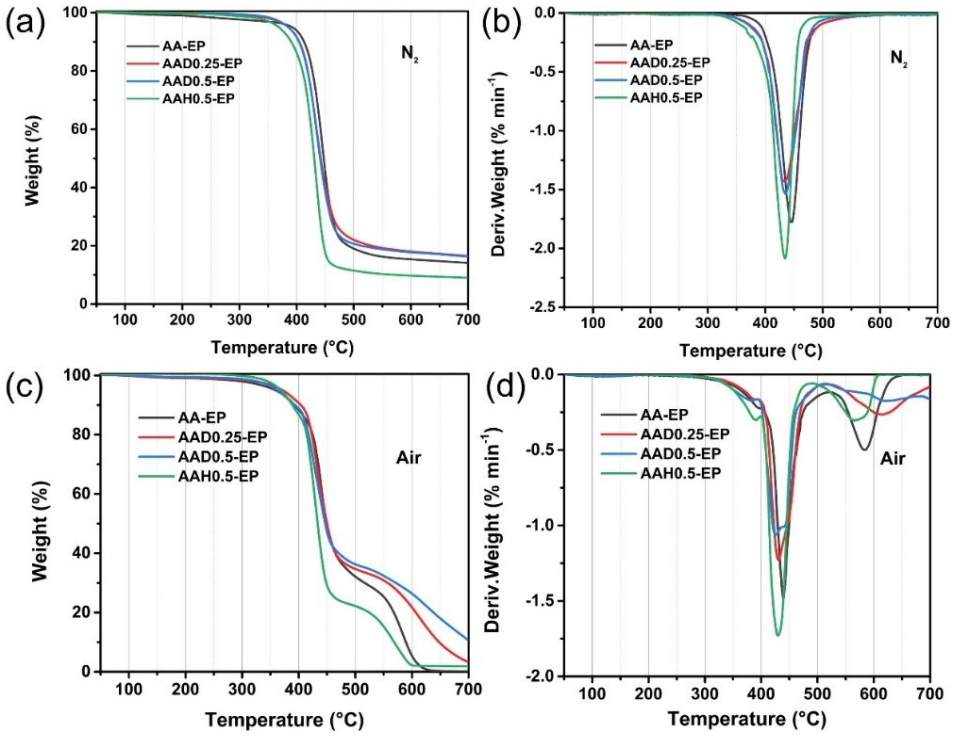


**Fig. S6** TG (a, c) and DTG curves (b, d) of AA-EP, AAD-EP and AAH0.5-EP in $N_2$ and air atmospheres.

## 8. Fire safety

Fire-safe results of the cured AA-EP, AAD-EP and AAH0.5-EP samples were collected in Table

S3; and the fire-safe results of the relevant CF composites were collected in Table S4.

**Table S3.** Fire-safe results of AA-EP, AAD-EP and AAH0.5-EP.

| Samples | AA-EP | AAD0.25-EP | AAD0.5-EP | AAH0.5-EP |
|---|---|---|---|---|
| TTI (s) | 65 | 69 | 56 | 58 |
| PHRR ($kW \cdot m^{-2}$) | 900.8 | 582.2 | 451.8 | 960.2 |
| THR ($MJ \cdot m^{-2}$) | 66.2 | 52.6 | 33.2 | 77.7 |
| TTPHRR (s) | 125 | 115 | 90 | 125 |
| FIGRA ($kW \cdot m^{-2} \cdot s^{-1}$) | 8.1 | 5.4 | 5.1 | 8.4 |
| MAHRE ($kW \cdot m^{-2}$) | 286.7 | 205.1 | 155.6 | 311.6 |
| Av-EHC ($MJ \cdot m^{-2}$) | 21.6 | 15.3 | 15.1 | 21.2 |
| Residue (%) | 3.2 | 11.4 | 12.4 | 3.9 |
| LOI (%) | 22 | 34.5 | 36 | 23.5 |
| UL-94 | no rating | V-1 | V-0 | no rating |

**Table S4.** Fire-safe results of the EP/CF, AAD0.5-EP/CF and AAD0.5-EP.

| Samples | TTI (s) | PHRR ($kW \cdot m^{-2}$) | THR ($MJ \cdot m^{-2}$) | Residue (wt%) | LOI (%) | UL-94 |
|---|---|---|---|---|---|---|
| EP/CF | 22 | 431.0 | 69.5 | 31.5 | 27.5 | no rating |
| AAD0.5-EP/CF | 28 | 221.6 | 31.6 | 63.4 | 41.5 | V-0 |
| AAD0.5-EP | 56 | 463.3 | 33.2 | 12.4 | 36.0 | V-0 |

## 9. The mechanism of fire-safety

The digital photo and SEM micrographs of the burning residue of AAD-EP after cone calorimeter tests were provided, as shown in Fig. S7($a_1$-$a_4$). The AA-EP and AAH0.5-EP presented discontinuous appearance with numerous open holes on the surface, which was attributed to the emission of combustible volatiles during the combustion process, thus causing the exposure of EP

matrix to the heat flow outside and producing higher THR and PHRR values. In contrast, as the loading of DHH increased, the char surface got smoother and denser. The AAD0.5-EP owned the smoothest and densest residue char, indicating DHH with superior thermal resistance of the char layer mechanism. Raman spectroscopy was a method to assess the graphitization degree of char formed during burning, which was dependent on the intensity proportion of the D and G bands ($I_D/I_G$).[3] As showed in Fig. S7($b_1$-$b_4$), AA-EP presented the highest $I_D/I_G$ value for 2.02, whereas the $I_D/I_G$ values were reduced as the loading of DHH increased. The AAD0.5-EP exhibited the lowest $I_D/I_G$ value for 1.50 among all the samples, indicating the formation char residue with the highest graphitization degree and the most stable property.

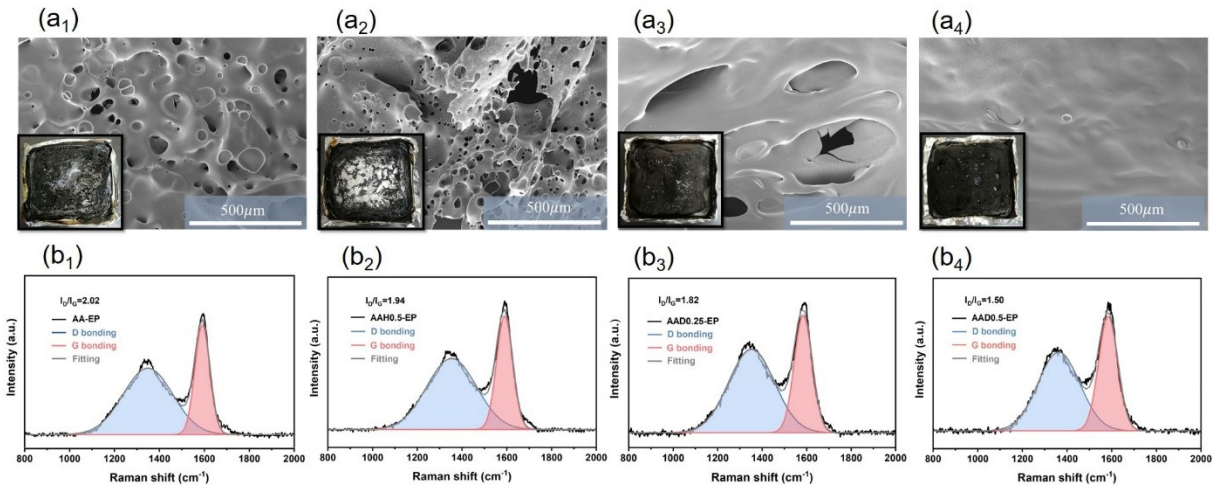


**Fig. S7** The digital photo and SEM micrographs of the residues after cone calorimeter tests, AA-EP ($a_1$), AAH0.5-EP ($a_2$), AAD0.25-EP ($a_3$) and AAD0.5-EP ($a_4$); the Raman spectra of the char residues after cone calorimeter tests, AA-EP ($b_1$), AAH0.5-EP ($b_2$), AAD0.25-EP ($b_3$) and AAD0.5-EP ($b_4$).

TG-FTIR (Fig. S8) was applied to investigate the volatile gas products of the AAD0.5-EP and AAH0.5-EP under the programmed heating process. During heating process, some phosphorus-containing fragments finally appeared in volatile products of AAD0.5-EP, suggesting DHH with positive flame-retardant activity in gaseous phase.

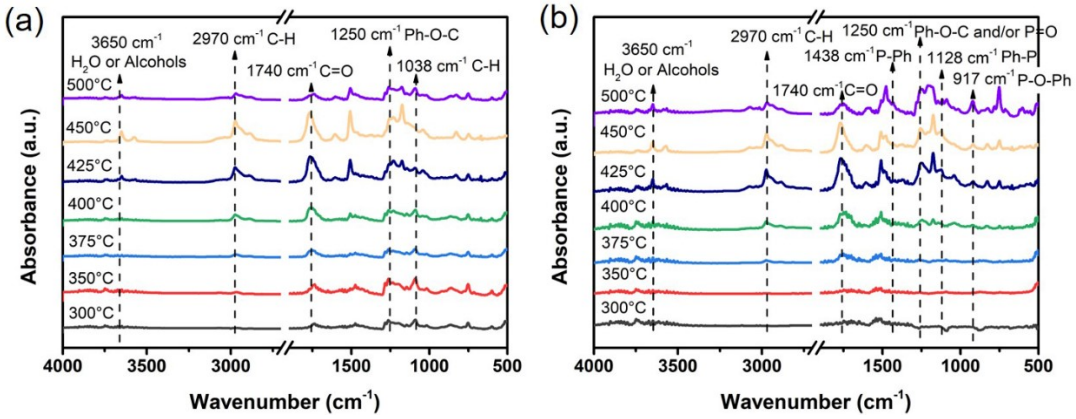


**Fig. S8** FTIR spectra of the volatile products for AAH0.5-EP (a) and AAD0.5-EP (b) at different temperatures.

## 10. The transesterification model compound

The synthetic process of the model compound (Fig. S9). The 1 eq. of octanoic acid (Aladdin, Industrial Co., Ltd) and the 1 eq. of phenylglycidyl ether (Aladdin, Industrial Co., Ltd) were mixed into a glass flask equipped with a magnetic stirrer. The synthesis was conducted at 120°C for 1.5h, and 2-MI (0.06 eq.) as a catalyst was added to promote the epoxy-acid esterification reaction. The products were used directly as synthesized without further purification. $^{1}$H NMR (400 MHz, DMSO-$d_6$) δ 7.34-7.23 (m, 2H), 6.93 (ddt, J = 7.3, 2.8, 1.6 Hz, 3H), 5.81 (s, 1H), 4.42-3.72 (m, 5H), 2.30 (td, J = 7.3, 3.9 Hz, 2H), 1.57-1.45 (m, 2H), 1.32-1.11 (m, 8H), 0.91-0.78 (m, 3H).

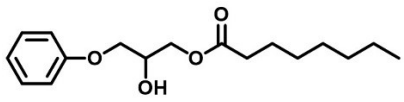


**Fig. S9** The chemical structure of molecule model compound 1.

## 11. The reprocessability

The reprocessability of the fire-safe vitrimers through compression molding at 220 °C under

different reprocessed pressure were discussed.

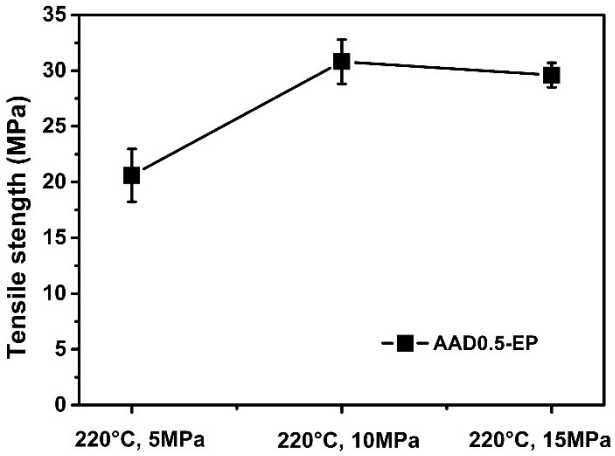


**Fig. S10** The tensile strength of AAD0.5-EP under different reprocessing pressure.

The SEM images of the tensile fracture surfaces of the recycled AAD0.5-EP at 220 °C under 10 MPa for different reprocessing times-were illustrated in Fig. S11. Comparison of the mechanical property, recycling efficiency and fire-safe parameters of different epoxy vitrimers in literatures were summarized in Table S5; while the cone calorimetric results of the original and recycled AAD0.5-EP were listed in Table S6. SEM micrographs and merged EDX elemental mapping images of the burning residues of the original and recycled AAD0.5-EP after cone calorimetry were shown in Fig. S12.

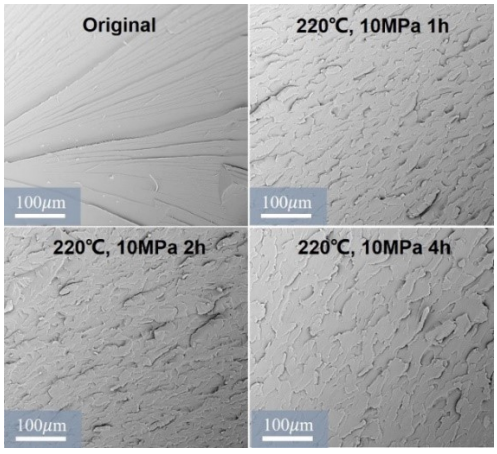


**Fig. S11** SEM images of the tensile fracture surfaces of the recycled AAD0.5-EP under different

reprocessing time.

**Table S5.** Comparison of the mechanical property, recycling efficiency and fire-safe parameters of different epoxy vitrimers in literatures.

| Reference | transesterification catalyst | $\sigma_0$ (MPa) | $\sigma_R$ (MPa) | Recycling efficiency (%) | LOI (%) | UL-94 |
|---|---|---|---|---|---|---|
| 6c | No | 11.0 | 9.1 | 82.6 | - | - |
| 7c | No | 2.6 | 2.5 | 96.2 | - | - |
| 9a | Yes | 41.3 | 41.3 | 100 | - | - |
| 9b | No | 31.6 | 27.0 | 85.4 | - | - |
| 23a | No | 43.2 | 42.8 | 99.1 | - | - |
| 23b | Yes | 41.2 | 31.0 | 75.2 | - | - |
| 23c | No | 28.7 | 28.0 | 97.5 | 30.5 | V-0 |
| 23d | Yes | 46.0 | 41.0 | 89.1 | - | - |
| Our work | No | 69.0 | 30.8 | 44.6 | 36 | V-0 |

**Table S6.** Cone calorimetric results of the original and recycled AAD0.5-EP.

| Samples | AAD0.5-EP | Recycled-AAD0.5-EP |
|---|---|---|
| TTI (s) | 56 | 59 |
| PHRR ($kW \cdot m^{-2}$) | 463.3 | 468.2 |
| THR ($MJ \cdot m^{-2}$) | 33.2 | 40.9 |
| TTPHRR (s) | 90 | 110 |
| FIGRA ($kW \cdot m^{-2} \cdot s^{-1}$) | 5.1 | 4.3 |
| MAHRE ($kW \cdot m^{-2}$) | 155.6 | 190.7 |
| Residue (%) | 12.4 | 19.9 |
| LOI (%) | 36 | 36 |
| UL-94 | V-1 | V-0 |

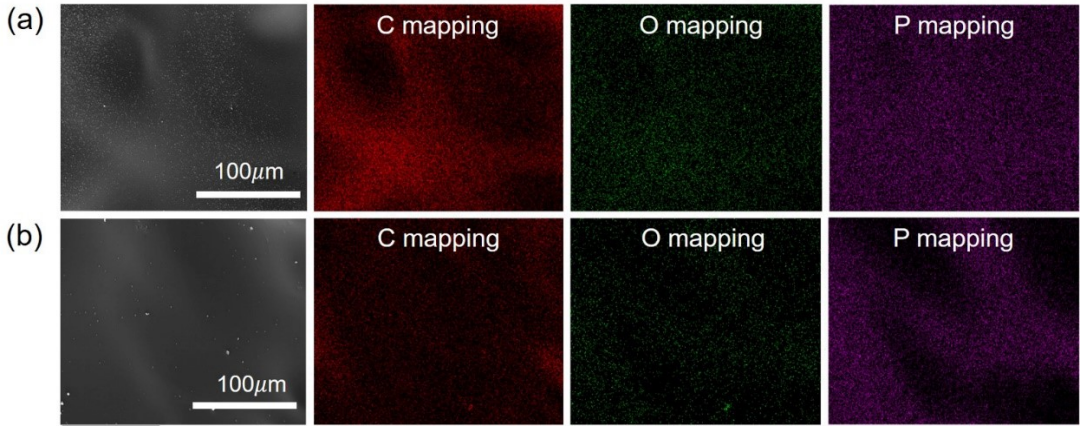


**Fig. S12** SEM micrographs and merged EDX elemental mapping images (C, O and P in red, green and violet signal, respectively) of burning residues of original (a) and recycled (b) AAD0.5-EP after cone calorimetry.

## 12. The repairing

The AAD0.5-EP was cut to two fragments using a knife, placed between two metal plates, and then placed in an oven at 200 °C for 1h. Then, the repairing (welding) behavior was evaluated by testing the stress-strain performance the original and thermally welding AAD0.5-EP samples, as shown in Fig. S13.

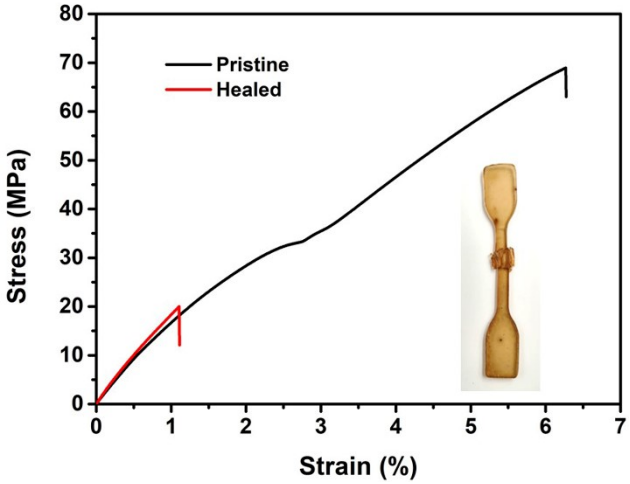


**Fig. S13** The stress-strain curves of the original and thermally welding AAD0.5-EP samples.

## 13. The alcoholysis process

The alcoholysis process was that AAD0.5-EP was immersed in EG solution for 5h and achieve the completely dissolution (Fig. S14(a)). The chemical structures of the degradation products (I/II/III) were confirmed by MS in Fig. S14(b) and (c), as shown below.

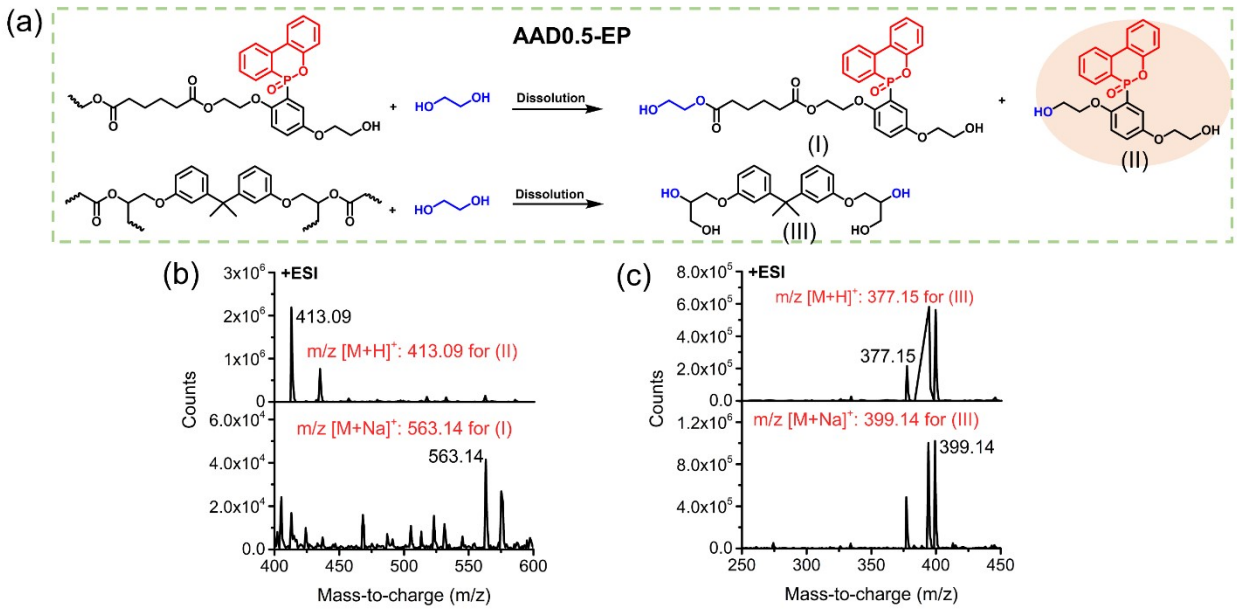


**Fig. S14** Solvolysis of AAD0.5-EP in EG. (a) Alcoholysis processes of different ester-linkages. (b) and (c) the MS analysis of the degradation products (I/II/III).

## References


[1] C. S. Wang, C. H. Lin, C. Y. Chen, *J. Polym. Sci., Part A: Polym. Chem.* 1998, **36**, 3051-3061.

[2] a) X.-L. Zhao, Y.-Y. Liu, Y. Weng, Y.-D. Li, J.-B. Zeng, *ACS Sustain. Chem. Eng.* 2020, **8**, 15020-15029;

b) Y.-F. Lei, X.-L. Wang, B.-W. Liu, X.-M. Ding, L. Chen, Y.-Z. Wang, *ACS Sustain. Chem. Eng.* 2020, **8**, 13261-13270.

[3] a) Y. Fang, J. Miao, X. Yang, Y. Zhu, G. Wang, *Chem. Eng. J.* 2020, **385**, 123830;

b) J.-N. Wu, L. Chen, T. Fu, H.-B. Zhao, D.-M. Guo, X.-L. Wang, Y.-Z. Wang, *Chem. Eng.*

*J.* 2018, **336**, 622-632.